Biointerface Research in Applied Chemistry
Platinum Open Access Journal (ISSN: 2069-5837)

Article
Volume 12, Issue 1, 2022, 264 - 278
https://doi.org/10.33263/BRIAC121.264278

Molecular Docking and Extended Spectroscopy to Binding Characterizations: Etoposide a Glycoside of Podophyllotoxin with Bovine Serum Albumin

Manjushree Makegowda [1], Revanasiddappa Hosakere Doddarevanna [2,*]

[1] Department of Chemistry, MMK & SDM Mahila Mahavidyalaya, Krishnamurthypuram, Mysuru 570 004, Karnataka, India; mmanjushreem@gmail.com (M.M.);
[2] Department of Chemistry, University of Mysore, Manasagangothri, Mysuru 570 006, Karnataka, India; hdrevanasiddappa@yahoo.com (R.H.D.);
* Correspondence: hdrevanasiddappa@yahoo.com;

Scopus Author ID 7004879365
Received: 26.02.2021; Revised: 1.03.2021; Accepted: 6.04.2021; Published: 20.04.2021

Abstract: A significant soluble protein, specifically bovine serum albumin (BSA) plays an efficient role in drug delivery, and etoposide (ETS) is used to cure various cancers. Binding interaction between ETS and BSA examined by 3D, emission, synchronous fluorescence's, UV–vis, FT–IR, and CD spectroscopy's in the association of computational at pH 7.40 with 293, 301 and 309 K. Formed complex between ETS and BSA dominates van der Waals and bonding of hydrogen's at sub-domain IIIA. Strong binding of ETS−BSA leads to altering BSA's structural and conformations statically. Energy transfer reveals ETS−BSA distance. Apart from this, ETS−BSA binding is affected by Mg^{2+}, Cu^{2+}, Fe^{2+}, $Ca^{2+,}$ and Co^{2+} ions. This study may help in the drug development and discovery process.

Keywords: etoposide; bovine serum albumin; anti-cancer; molecular docking; circular dichroism.

1. Introduction

Etoposide (ETS) belonging to topoisomerase II inhibitor and plant alkaloid classifications where it is cytotoxic and antineoplastic named as anti-cancer (Figure 1A) [1]. It is podophyllotoxin semisynthetic derivative exhibiting antitumor activity with IUPAC name (5S,5aR,8aR,9R)-5-[[(2R,4aR,6R,7R,8R,8aS)-7,8-dihydroxy-2-methyl-4,4a,6,7,8,8a-hexahydropyrano[3,2-d][1,3]dioxin-6-yl]oxy]-9-(4-hydroxy-3,5-dimethoxyphenyl)-5a,6,8a,9-tetrahydro-5H-[2]benzofuro[6,5-f][1,3]benzodioxol-8-one with PubChem CID 36462. ETS is sometimes employed in bone marrow or blood stem cell transplantation. It is frequently combinational use with bleomycin to treat testicular cancer. ETS forms a ternary complex with topoisomerase II enzyme and DNA by inhibiting DNA synthesis and breaking DNA strands to prevent topoisomerase II binding repair. Cell death is caused by massed DNA breaks preventing entry to cell division of mitotic phase [2-4].

Several biological systems (biology, immunology, pharmacology, etc.) and medical sciences considering the interaction of proteins (bio-macromolecules) with drugs, hormones, fatty acids, etc. (small molecules): Moreover, these investigations nowadays becoming interest and vast field to modulate properties of drugs in pharmacodynamic and pharmacokinetics. Due to changes caused by proteins' structure, their functioning was also affected by drug molecule interaction [5].

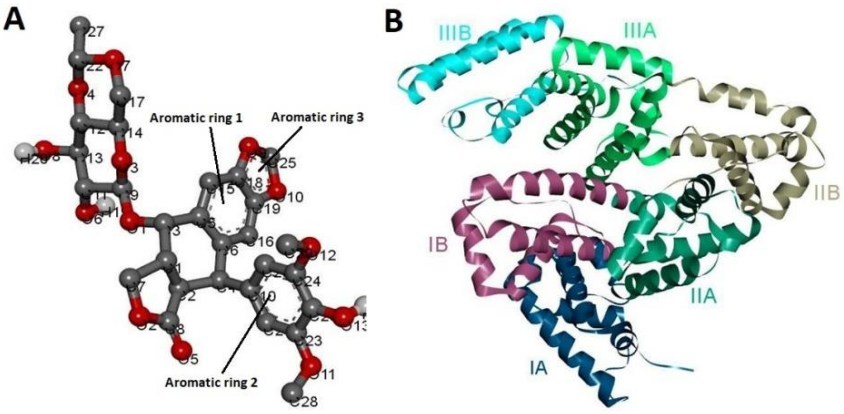

Figure 1. (A) Etoposide (ETS) and (B) bovine serum albumin (BSA) by Discovery Studio 3D picturing.

BSA (bovine serum albumin) (Figure 1B), among assorted serum albumins, a highly abundant, soluble, and easily obtainable at low cost extracellular globular protein, comprised with 2 tryptophans (Trp), a free thiol, and 17 disulfide bridges from 583 amino acids [6] of single polypeptide synthesized in the liver and exhibiting phenomenal ligand binding properties [7].

Drug-protein binding interfered with by metal ions available (either already inside or taken from outside through any means) in the body, and hence, drug therapeutic effect inflection occurs by diminishing its free concentration. These metal ions are offered by several sites on proteins for binding with unlike specificities and act similar to their sequestration agents [8]. Hence, drug-protein binding emerges imperative to rationalize by variant metal ions presence.

This work aspires to critique ETS's effect on BSA to estimate binding affinity, monitor BSA structural variations, and course of interaction. For this, manifold spectroscopy in unification with docking techniques has been exerted. Effect of Mg^{2+}, Cu^{2+}, Fe^{2+}, $Ca^{2+,}$ and Co^{2+} ions have been envisaged on ETS−BSA binding in a proposed report.

2. Materials and Methods

2.1. Materials and stock solutions.

Sigma-Aldrich (USA) products: BSA (A1933, ≥98%), ETS (E1383, 98.0-105.0%), magnesium chloride hexahydrate (M2670, ≥98%), copper(II) sulphate pentahydrate (209198, ≥98%), iron(II) sulphate heptahydrate (215422, ≥99%), calcium chloride (C1016, ≥93.0%), cobalt chloride hexahydrate (769495, ≥97%), warfarin (258016, 98%), ibuprofen (I4883, ≥98%) and digitoxin (D5878, ≥92%) were utilized and other reagents entirely of analytical grade. Warfarin, ibuprofen, digitoxin, metal ions, and ETS were stock solutions at 1.0 $\times 10^{-3}$mol L^{-1} whereas BSA at 1.0 $\times 10^{-4}$mol L^{-1}. Double-distilled water made used for Tris buffer (NaCl: 0.15 M and Tris: 0.05 M at pH 7.40) preparations wherein throughout whole experiments capitalized the Tris buffer and corrected its background to each measurement.

2.2. FT−IR analysis.

Infrared spectra were examined on Perkin Elmer FT−IR spectrometer Spectrum Two (USA) enhanced with OptKBr beam splitter, deuterated-triglycine sulfate detector, and germanium accessory as ATR (attenuated total reflection) for free BSA and ETS−BSA system at 301 K. Further, 4 cm^{-1} resolution at 1700−1500 cm^{-1} and 90 scans were claimed while

recording infrared spectra. Free BSA and ETS−BSA system secondary structure evaluations are determined from amide I band shape, located around 1700−1600 cm^{-1}. By the second derivative resolved the major peaks [9], and this was subjected to the curve-fitting method for deconvolution measured with Gaussian function. Concentrations of both ETS and BSA kept at 8.4×10^{-6}mol L^{-1}.

2.3. Circular Dichroism (CD).

To analyze the BSA (4.2×10^{-6}mol L^{-1}) secondary structure alterations, CD spectra were taken at 200−240 nm (301 K) without and with ETS (105×10^{-6}mol L^{-1}) on a JASCO CD spectropolarimeter (J-815 Japan) with scan speed 100 nm/min and cell length 10 mm. To compute the secondary structural percentage of BSA without and with ETS, BeStSel online software was used.

2.4. UV−visible measurements.

A wavelength of 200−300 nm was applied to UV−vis spectra on DU 730 Beckman Coulter UV−visible Spectrophotometer (U.S.A.) to BSA (4.2×10^{-6}mol L^{-1}) with ETS different concentrations 0.0, 0.7 up to 7.0 ($\times 10^{-6}$mol L^{-1}).

2.5. Fluorescence emission spectroscopy.

At 293, 301, and 309 K, fluorescence measurements exploited to BSA (4.2×10^{-6}mol L^{-1}) in various ETS amounts (0.0 to 7.0×10^{-6}mol L^{-1}) on Hitachi fluorescence spectrophotometer F-4600 (Japan) with Xenon lamp (150 W). Excitation/emission slit widths were 10/10 nm, wavelength range 295−425 nm and λ_{ex} = 295 nm. External circulatory water bath maintains the expected temperatures. Effect of the inner filter was annihilated from fluorescence intensities (F_{cor} = corrected and F_{obs} = observed) by recording the ETS absorbance at wavelengths of excitation (A_{ex}) and emission (A_{em}) using equation (1):

$$F_{cor} = F_{obs} \times e^{(A_{ex} + A_{em})/2} \quad (1)$$

2.6. Three-dimensional fluorescence (3D).

BSA at 4.2×10^{-6}mol L^{-1} and ETS at 126×10^{-6}mol L^{-1} were used to obtain the free BSA and ETS−BSA system fluorescence 3D spectra (1:30 molar ratio) at 301 K. The monitored wavelengths were excitation at 200−380 nm and emission at 250−500 nm.

2.7. Synchronous fluorescence.

Synchronous spectra were obtained for the ETS−BSA system to achieve Tyr and Trp microenvironments where wavelengths of excitation and emission were scanned simultaneously between 240 to 320 nm (Tyr) 210 to 250 nm (Trp) at 301 K. Concentrations of BSA and ETS used were similar to emission fluorescence.

2.8. Molecular docking.

Molecular docking analysis was executed on Autodock Tools 1.5.6 along with Autodock 4.2 as well as Autogride 4.2 [10]. BSA crystal structure with resolution at 2.5 Å was made use from Protein Data Bank with id 3V03, and energy minimization was brought about

on Swiss-Pdb Viewer and force field GROMOS96 (43B1). Marvin View was facilitated to build a 3D structure of ETS followed by minimization of energy. Each binding site (I, II, and III) independently docked for ETS with 250 iterations and respective 3D coordinates. For conformational searching, the genetic algorithm of Lamarckian was employed at 250000 energy evaluations, and the ETS docking modes were clustered on RMSD cut-off base at tolerance 2.0 Å. Visualization of the ETS−BSA complex was exerted on Biovia Discovery Studio.

2.9. BSA to ETS distance analysis.

To examine BSA to ETS energy transfer, BSA (4.2×10^{-6}mol L^{-1}) fluorescence emission and ETS (4.2×10^{-6}mol L^{-1}) UV−visible absorption in 300−400 nm at 301 K overlapped.

2.10. Competitive site markers binding.

Binding displacement investigations through fluorescence emission were accomplished for BSA−ETS interaction in the existence of site markers such as for assistance warfarin, ibuprofen, and digitoxin respectively bind to sites I, II, and II. BSA and site markers concentrations were set at 4.2×10^{-6}mol L^{-1}, while the concentration of ETS gradually varied between 0 and 7.0×10^{-6}mol L^{-1} at 301 K.

2.11. Metal ions significances on ETS−BSA system.

Influence of Mg^{2+}, Cu^{2+}, Fe^{2+}, Ca^{2+} and Co^{2+} ions on ETS binding to BSA wasanalyzed by recording fluorescence data by varying the ETS concentrations (from 0.0 to 7.0×10^{-6}mol L^{-1}) with BSA and metal ions (4.2×10^{-6}mol L^{-1}) constant at 301 K in 295−425 nm.

2.12. Statistical analysis and evaluations of results.

All experiments proceeded 3 times, and actual data were obtained from mean $\pm$ standard deviation (SD) where data interpretations were made on OriginPro 9.0 and Microsoft Excel.

3. Results and Discussion

3.1. FT−IR study.

Figure 2 depicts free BSA and ETS−BSA system FT−IR spectral shift at amide I (C=O stretching) and amide II 1600−1500 cm^{-1} (C−N stretch joined N−H bend) [11]. Modification of BSA with and without ETS in spectral intensities epitomizes ETS interaction with BSA (Table 1). Besides, compared information for free BSA and ETS−BSA system on distinct kind of secondary structures signifies the decrease of α-helix, random coil and β-sheet with an increase in the β-turn and β-antiparallel from (Figure 3 and Table 2) were observed. This comes out with BSA secondary structure changes that provoke partial unfolding of BSA in ETS presence.

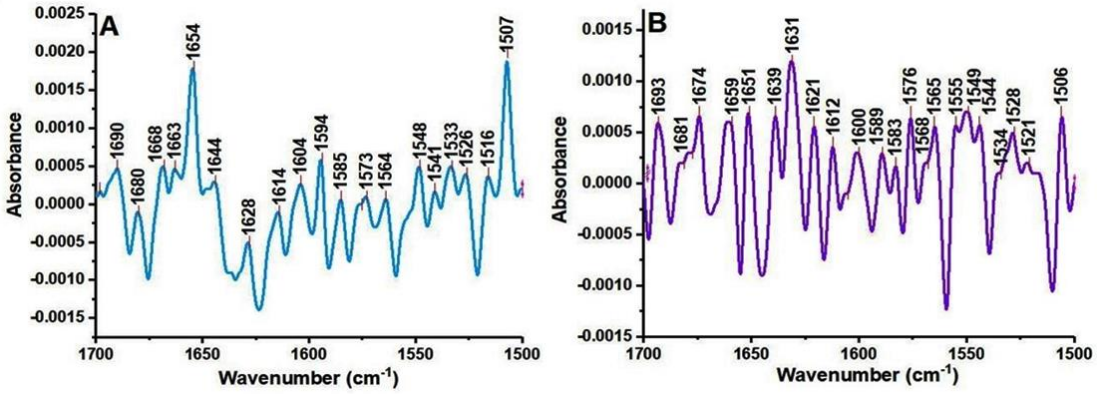

Figure 2. FT−IR spectra at 301 K for (A) free BSA and (B) ETS−BSA system where concentrations of ETS and BSA were each at 8.4×10^{-6}mol L^{-1}.

Table 1. Free bovine serum albumin and etoposide−bovine serum albumin system at 301 K: Positing of peaks in Fourier transform−Infrared spectra

System	Amide I (cm^{-1})					Amide II (cm^{-1})
	1615-1637	1638-1648	1649-1660	1660-1680	1680-1692	1548
Free BSA	1628 ± 0.78	1644 ± 0.61	1654 ± 0.46	1680 ± 0.79	1690 ± 0.16	1548 ± 0.94
ETS−BSA	1621 ± 0.56	1639 ± 0.28	1651 ± 0.67	1674 ± 0.60	1681 ± 0.29	1544 ± 0.85

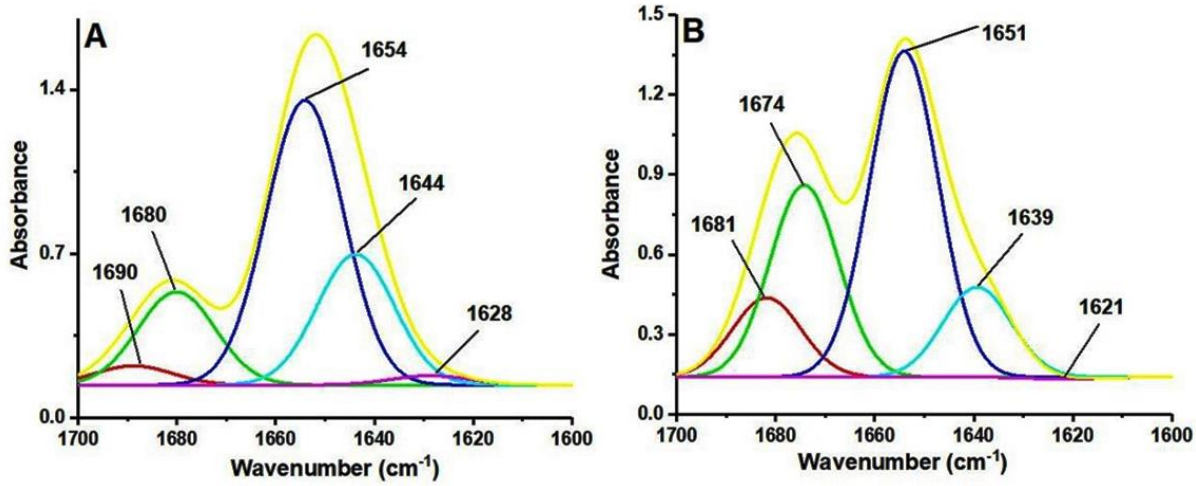

Figure 3. Curve fitting analysis to amide I band (A) Bovine serum albumin alone and (B) etoposide −bovine serum albumin system employed with Gaussian peak function by second derivative resolution.

Table 2. FT−IR and CD study for ETS and BSA interaction to the secondary structure at 301 K.

	System	Secondary structures (%)				
		β-sheet	Random coil	α-helix	β-turn	β-antiparallel
FT−IR	Free BSA	1.74 ± 0.07	24.33 ± 0.10	53.03 ± 0.04	17.34 ± 0.04	3.56 ± 0.06
	ETS−BSA	0.65 ± 0.08	13.08 ± 0.09	47.41 ± 0.07	27.32 ± 0.06	11.54 ± 0.07
CD	Free BSA	3.78 ± 0.04	23.69 ± 0.06	55.40 ± 0.01	14.99 ± 0.09	2.06 ± 0.02
	ETS−BSA	1.02 ± 0.05	12.61 ± 0.09	48.53 ± 0.03	25.46 ± 0.08	12.38 ± 0.01

3.2. CD spectroscopy.

To examine the secondary structural alteration [12] due to ETS binding to BSA, CD spectra were obtained having 2 minima for transitions $\pi \rightarrow \pi^*$ (208 nm) and $n \rightarrow \pi^*$ (222 nm) intimating the presence of α-helical structure dominantly. Band maxima of two negative intensities of peaks were decreased for free BSA on ETS addition without shift, as depicted in Figure 4A. Table 2 suggesting the decrement of α-helix, β-sheet and random coil content with increment in β-antiparallel and β-turn content of free BSA upon ETS interaction. Therefore, ETS causes the BSA secondary structural modifications.

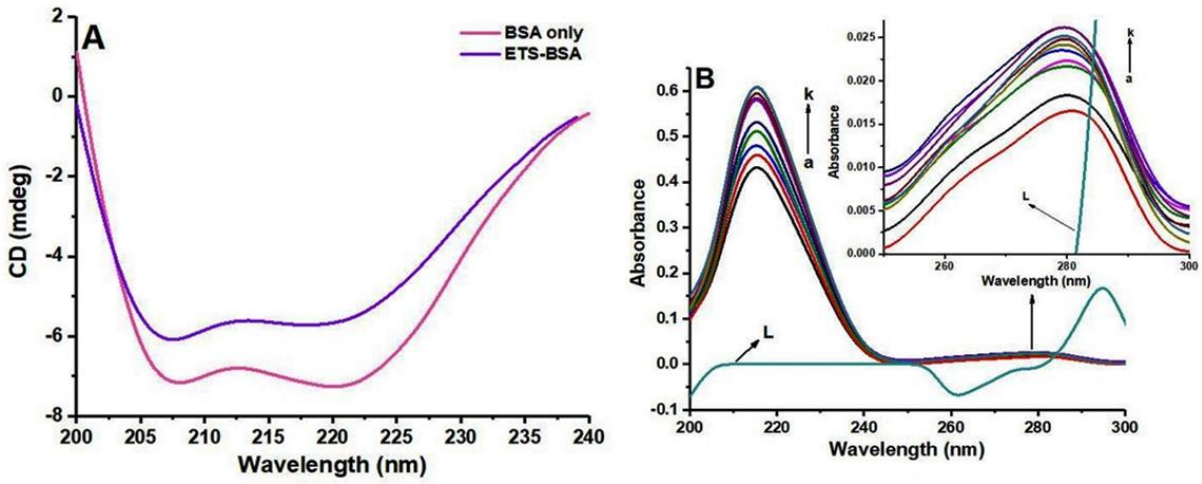

Figure 4. ETS−BSA system:(A)CD and (B) UV−visible spectra.

3.3. UV−vis absorption measurements.

To analyze the complex formation, estimations of UV−vis absorption area best and basic strategy. It is an adaptable system helpful for providing manifestation on small molecular binding to a macromolecule. The observed BSA absorption spectrum (Figure 4B) with ETS increased concentration increases the peak intensity by exposing two bands around 280 nm for aromatic amino acids (Tyr and Trp) and 210 nm (peptide groups) with a small redshift at both the peak positions [13]. This Suggesting ETS bound with BSA and formed a complex. Moreover, the shift of positioning peaks suggests that peptide groups and aromatic amino acids microenvironments alter.

3.4. BSA emission fluorescence characteristics.

Fluorescence spectra often give a qualitative analysis of ligand bind to BSA it caused by intrinsic flavors, specifically tryptophan (Trp), phenylalanine (Phe), and tyrosine (Tyr). In most cases, Tyr quenched completely when it around groups (carboxyl, amino, or Trp), then only Trp alone mainly causes intrinsic fluorescence. The addition of different ETS concentrations decreases the BSA emission fluorescence with redshift at 341 nm (λ_{ex} = 295 nm) (Figure 5A) signifying Trp is involved in this interaction, and it moves to a more polar environment.

A decrease in BSA quantum yield called fluorescence quenching is caused by various molecular interactions from fluorophore present in BSA. Static (formation of the fluorophore−quencher complex) and dynamic (fluorophore and quencher meet at excited state) are the two predominant quenching mechanisms that differ by temperature. At higher temperatures, diffusion increases, and the stability of the complex decreases. Hence, bimolecular quenching constants decrease for static increases for dynamic. Stern−Volmer equation (2) [14] was applied to fluorescence data of the BSA−ETS system.

$$F_0/F = 1 + k_q\tau_0[Q] = 1 + K_{SV}[Q] \quad (2)$$

$$k_q = K_{SV}/\tau_0 (3)$$

where, F_0 and F are BSA with and without ETS fluorescence intensity, respectively. k_q, $[Q]$, τ_0 and K_{SV} are quenching rate constant, ETS concentration, BSA average lifetime without ETS

(2.7×10^{-9} s) and Stern–Volmer quenching constant. Stern−Volmer plot (Figure 5B) and Table 3 demonstrate that a rise in temperature k_q and K_{SV} values were decreased. However, obtained k_q is of order 10^{13}L mol^{-1}s^{-1} which is greater compared to biopolymer with different quenchers for dynamic (2.0×10^{10}L mol^{-1}s^{-1}) [15]. This constitutes static quenching. Stern−Volmer equation (4) [16] in modified forms were further utilized to suspect a section of fluorophore accessible (f_a) and effective static quenching constant (K_a):

$$F_0/(F_0 - F) = (1/f_a) + (1/K_a f_a[Q]) \quad (4)$$

Figure 5C is the plot of modified Stern−Volmer purporting K_a, as its values were decreased at higher temperatures like K_{SV} (Table 3) . Static quenching again confirmed.

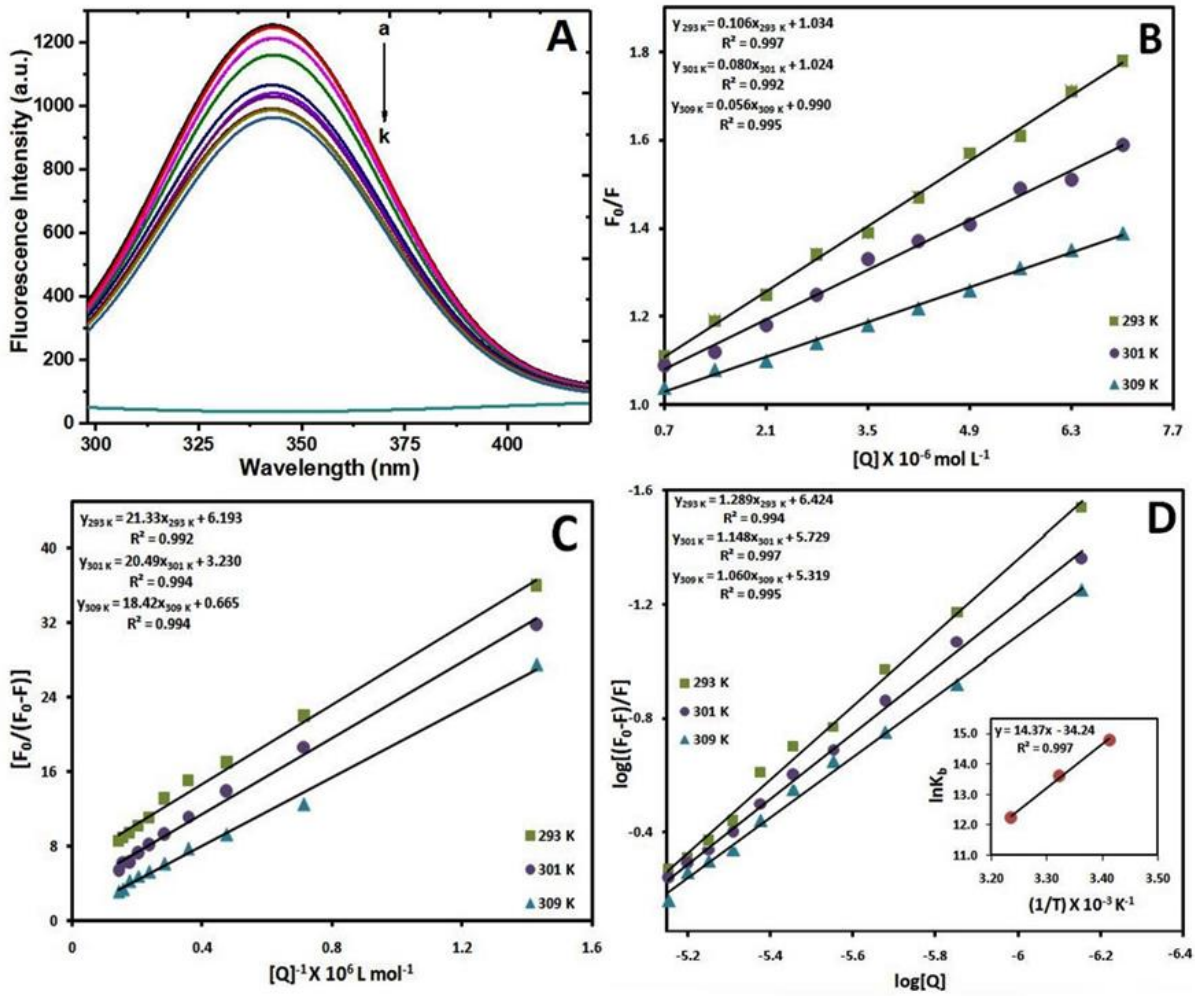

Figure 5. ETS−BSA system: (A) fluorescence emission spectra, (B) Stern−Volmer plot, (C) Modified Stern−Volmer plot, (D) plot for binding parameters and inset of (D) is van't Hoff plot at 293, 301, and 309 K.

Table 3. Stern−Volmer, rate and effective static quenching constants at different temperatures for ETS−BSA system.

Compound	Temperature (K)	K_{SV}(L mol^{-1}) × 10^{5} [a]	k_q (L mol^{-1}s^{-1}) × 10^{13} [b]	K_a (L mol^{-1}) × 10^{5} [c]
ETS−BSA	293	1.06 ± 0.07	3.92 ± 0.02	2.90 ± 0.08
	301	0.80 ± 0.06	2.96 ± 0.05	1.57 ± 0.07
	309	0.56 ± 0.04	2.07 ± 0.10	0.36 ± 0.03

[a]Stern−Volmer quenching constant, [b]quenching rate constant, and [c]effective static quenching constant

3.5. Binding parameters.

When small molecules independently bind to appropriate sites on macromolecules, Free and bound BSA with ETS exhibits equilibrium which is given by equation (5) [17]:

$$\log[(F_0 - F)/F] = \log K_b + n\log[Q] \quad (5)$$

According to equation (5), plot of $\log[(F_0 - F)/F]$ across $\log[Q]$ gives a slope and intercepts as binding site numbers (n) and $\log K_b$ at various temperatures (Figure 5D). The calculated values were outlined in Table 4, demonstrating the decreased K_b values increased at temperature raises resulting in partly decomposition of the formed complex at raised temperatures and an approximate value of n equal to 1, indicating only one ETS bind with BSA.

Table 4. Thermodynamic and binding parameters for ETS−BSA system at various temperatures.

Compound	Temperature (K)	K_b (L mol^{-1}) × 10^5 [a]	n^b	ΔG (k J mol^{-1})[c]	ΔH (k J mol^{-1})[d]	ΔS (J mol^{-1}K^{-1})[e]
ETS−BSA	293	26.55 ± 0.06	1.289	−36.06	−119.47	−284.67
	301	5.36 ± 0.01	1.148	−33.78		
	309	2.08 ± 0.05	1.060	−31.51		

[a]binding constant, [b]number of binding sites, [c]change is Gibb's free energy, [d]change in enthalpy, and [e]change in entropy

3.6. Thermodynamic explorations and binding forces.

In the solution phase, ligand and protein binding forces typically comprise van der Waals, hydrophobic, electrostatic, hydrogen bonds, etc. Predominant thermodynamic quantities used to examine the binding forces are change in enthalpy (ΔH), free energy (ΔG), and entropy (ΔS), which were related by van't Hoff equation (6):

$$\ln K_b = (-\Delta H/RT) + (\Delta S/R) \quad (6)$$

Where, K_b and R are binding constant at distinct temperatures T (293, 301, and 309 K) and gas constant. Plot of $\ln K_b$ opposite to $1/T$ using equation (6) gives ΔH and ΔS likewise equation (7) was applied to calculate ΔG are listed in Table 4 (placed inside Figure 5D). Ross and Subramanian [18] summed up binding forces for macromolecular interactions with small molecules through thermodynamic laws;

$$\Delta G = \Delta H - T\Delta S \quad (7)$$

It could be remarked from Table 3 that negative entropy and enthalpy values were indicative of hydrogen bonding and forces of van der Waals during BSA−ETS interaction as a major role. The estimated ΔG for the BSA−ETS complex is spontaneous and predominantly entropy-driven due to high esteem contrasted with enthalpy. And furthermore, all the assembled thermodynamics are negative, showing that this cooperation is exothermic.

3.7. 3D fluorescence measurements.

Characteristic parameters of free BSA and BSA−ETS system in 3D fluorescence spectra were exhibited in Figure 6 and Table 5. Peak '1' ($n \rightarrow \pi^*$ transition) was related to (Tyr and Trp residues) aromatic amino acids and peak '2' ($\pi \rightarrow \pi^*$ transition) displayed the polypeptide backbone. Peak 'a' ($\lambda_{em} = \lambda_{ex}$) refers to first-order and peak 'b' ($\lambda_{em} = 2\lambda_{ex}$) regards second-order scattering of Rayleigh [19]. All 4 peaks of BSA were significantly decreased when ETS was added. This result affirms that the ETS was formed a complex with BSA and induces the conformation alterations in BSA.

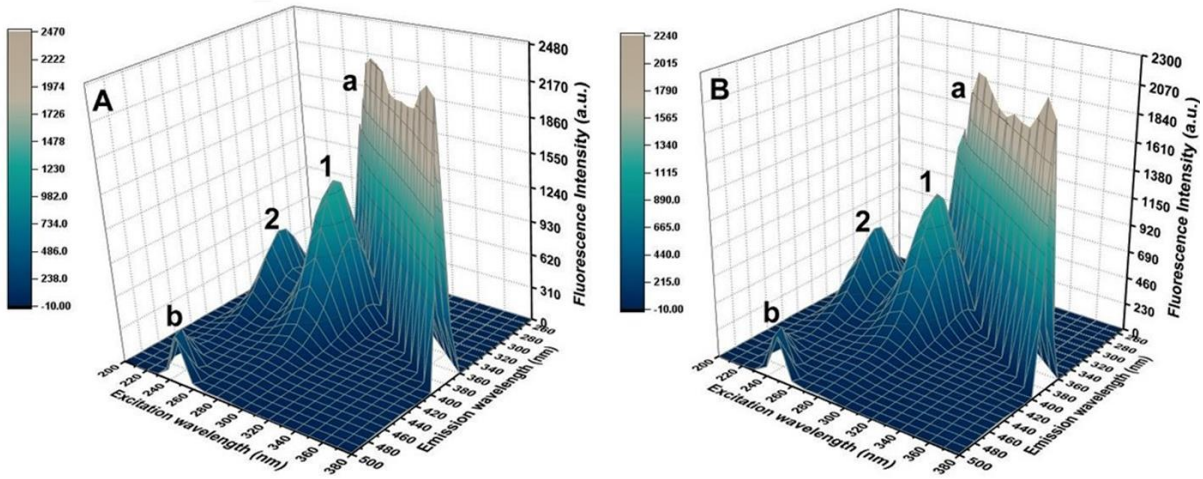

Figure 6. 3D fluorescence spectra at 301 K: (A) free BSA (4.2×10^{-6}mol L^{-1}) and (B) ETS−BSA system. ETS concentration was 126×10^{-6}mol L^{-1}.

Table 5. 3D fluorescence illustrations at 301 K.

Peak position ($\lambda_{ex}/\lambda_{em}$nm/nm)	Peak	Intensity	
		Free BSA	ETS−BSA
270/270 → 370/370	a	2159 → 2425	1780 → 2122
250/500	b	445.7	378.9
280/340	1	1336	1138
230/340	2	700.2	671.6

3.8. Synchronous fluorescence spectroscopy.

The molecular environment of chromospheres present in BSA after ETS interaction can be well examined from synchronous fluorescence. Wavelength difference ($\Delta\lambda$= excitation and emission) are devised at 15 and 60 nm for Tyr and Trp, respectively. It is viewable from Figures 7A and 7B that red shifts 3 nm were observed for Trp and no shifts for Tyr [20], indicating that microenvironments around Trp disturbed and the polarity was increased for the BSA−ETS system.

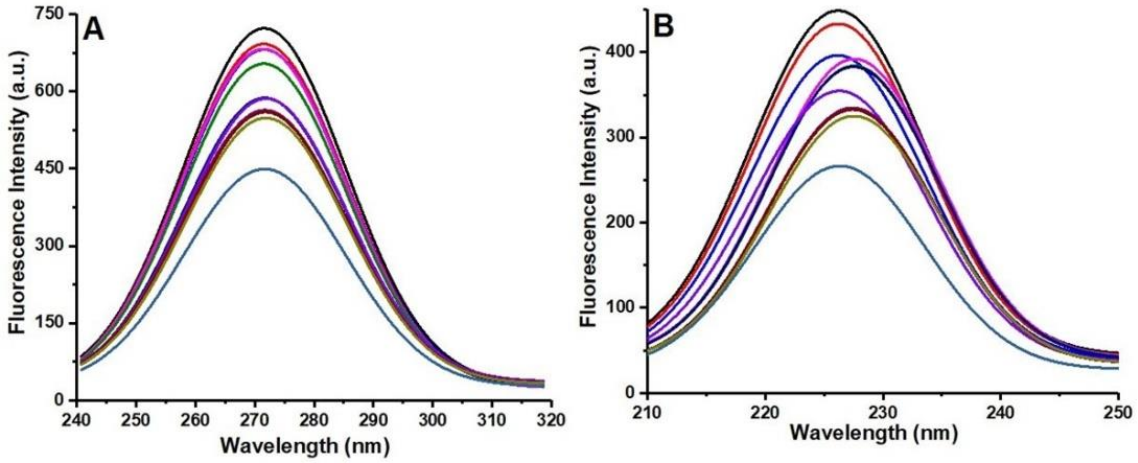

Figure 7. Synchronous fluorescence spectra to (A)Tyr ($\Delta\lambda$ = 15 nm) and (B) Trp ($\Delta\lambda$ = 60 nm) present in BSA (4.2×10^{-6}mol L^{-1}) with various ETS (0.0×10^{-6} to 7.0×10^{-6}mol L^{-1}) quantities at 301 K.

3.9. Molecular docking analysis.

Site-defined docking analysis computationally was performed to obtain the favorable binding mode of ETS among three binding sites on BSA. From the determined binding modes, the free energies of different binding sites of ETS were compared. Subsequent binding analyses

for each binding site were described in Figure 8, Table 6, and Table 7, representing amino acid residues, distances, and type of interaction of BSA after ETS interaction. Cluster analysis reveals largest cluster 68 was found to consist of 66 (site I), 71 (site II), and 39 (site III) mode with respective mean binding energies in the order −27.42, −33.78, and −21.88 KJ mol^{-1}. Therefore, ETS seems to more preferably binding to site II i.e., IIIA sub-domain of BSA by largest cluster modes with smallest binding energy. Binding energies for site II at the top 5 graded are tabulated in Table 8. Polar and ionic nature amino acid residues dominantly participated in this binding process along with high negative $E_{vdw+HB+desol}$ value compared to E_{Elec} in form, the hydrogen bond and van der Waals is the predominant binding process towards the BSA−ETS complex stability. Theoretical calculations from fluorescence thermodynamics were following docking.

Table 6. ETS favorably binding to sub-domain IIIA of BSA by molecular docking representations.

Binding site	Interactions		Amino acid – ETS atom
	Type	Distance (Å)	
	Vander Waals	-	GLN389
		-	ASN390
		-	THR491
		-	ARG409
	Conventional Hydrogen Bond	2.21	ARG484: HH12 – O12
		2.43	ARG484:HH12 – O13
		1.71	LYS413:HZ1 – O6
		2.30	LEU490: O – H19
Site II (IIIA)		2.29	SER488: O – H19
	Carbon Hydrogen Bond	2.90	ASN385: OD1 – C28
		2.97	PRO485: O – C29
		2.58	LYS413: CE – O8
		3.32	PRO492: CD – O4
		2.77	SER488: CB – O12
	Alkyl	3.81	ARG412: (CG-CB) – C27
		3.38	PRO492: aromatic ring – C27
		4.47	ALA489: CB – (C1 – C7)
	Pi-Alkyl	5.06	LEU386: (CD2-CG-CD1) – aromatic ring 2

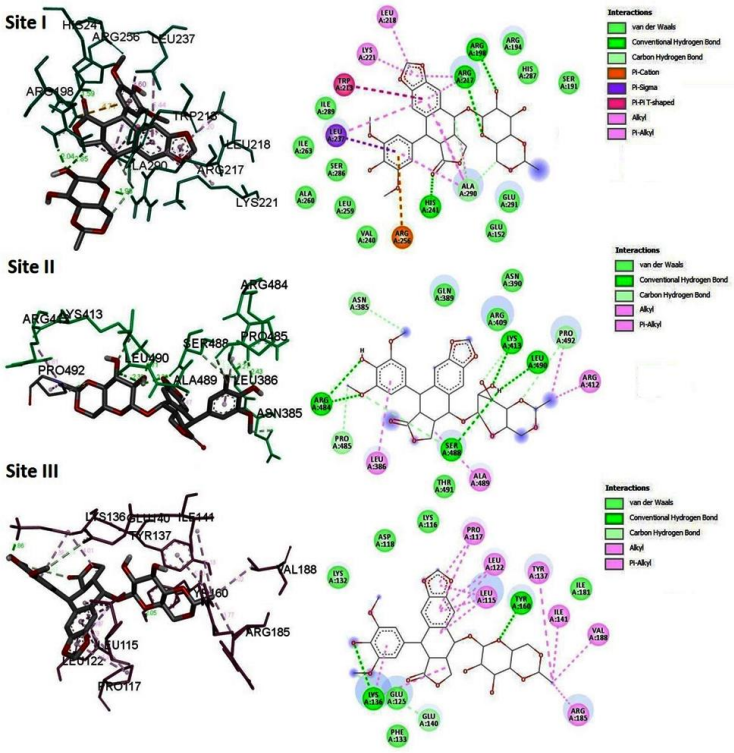

Figure 8. Molecular docking to ETS−BSA system at different sites.

Table 7. Binding characteristics for etoposide at sites I and III in bovine serum albumin by molecular docking.

Binding site	Interactions		Amino acid – ETS atom
	Type	Distance (Å)	
	vander Waals	–	ILE289
		–	ILE263
		–	SER286
		–	ALA260
		–	LEU259
		–	VAL240
		–	ARG194
		–	HIS287
		–	SER191
	Conventional Hydrogen Bond	1.59	HIS241:HE2 – O5
		1.98	ARG217: HH22 – O3
		2.85	ARG198: HH11 – O6
Site I (IIA)	Carbon Hydrogen Bond	3.52	ALA290: O – C3
		2.75	ALA290: O – C17
	Pi-Cation	4.71	ARG256:NH2 - aromatic ring 2
	Pi−Sigma	3.60	LEU237:CD1 − aromatic ring 2
	Pi-Pi T-Shaped	5.67	TRP213: aromatic ring − aromatic ring 2
	Pi-Alkyl	4.75	ALA290: CB − aromatic ring 1
		4.67	ALA290: CB − aromatic ring 2
		5.44	LEU237: CG − aromatic ring 1
		4.20	LEU218: CB - aromatic ring 3
		4.41	ARG217: (CB-CG) - aromatic ring 1
		3.48	ARG217: (CB-CG) − aromatic ring 2
		4.21	LYS221: (CG-CD) − aromatic ring 3
	Alkyl	3.71	ALA290: CB – (C5-C6)
		2.97	ALA290: CB – (C1-C7)
	Vander Waals	–	LYS116
		–	ASP118
		–	LYS132
		–	GLU125
		–	PHE133
		–	ILE181
	Conventional Hydrogen Bond	1.86	LYS136: HZ2 – O13
		2.05	TYR160: HH – O3
	Pi-Alkyl	5.40	TYR137: aromatic ring – C27
		4.38	LYS136: (CB-CG-CD) – aromatic ring 2
Site III (IB)		5.28	PRO117: (CD-CG-CB) – aromatic ring 1
		4.36	PRO117: (CD-CG-CB) – aromatic ring 3
		4.79	LEU122: (CD2-CG-CD1) − aromatic ring 1
		4.47	LEU115: (CB-CG-CD1) − aromatic ring 1
		4.53	LEU115: (CB-CG-CD1) − aromatic ring 2
	Alkyl	5.13	ILE141: (CG2-CB-CG1) – C27
		4.02	VAL188: (CG2-CB-CG1) – C27
		4.01	LYS136: (CB-CG-CD) – (C7-C1)
		4.73	LEU122: (CD2-CG-CD1) – (C6-C5)
		5.32	LEU115: (CB-CG-CD1) – (C6-C5)

3.10. Energy transfer between ETS and BSA.

Energy transfers from BSA to ETS occur when the bellow criteria are available: (i) BSA produces fluorescent light, (ii) overlap between fluorescence emission and absorbance spectrum of BSA and ETS, respectively, (iii) Their distances (r) should be lesser than 8 nm. Critical distance (R_0) also influences energy transfer (E) when it 50% in addition to r according to the theory of Föster's energy transfer,

$$E = R_0^6/(R_0^6 + r^6) = (F_0 - F)/F_0 \quad (8)$$

$$R_0^6 = 8.8 \times 10^{-25} K^2 N^{-4} \Phi J \quad (9)$$

K^2, N and Φ are constants of BSA comparative transition dipoles orientation in space, medium refractive index, and fluorescence quantum yield without ETS, respectively [21]. BSA emission and ETS absorption overlap integral J (Figure 9) was evaluated from equation (10):

$$J = \{\sum[F_d(\lambda)\varepsilon_a(\lambda)\lambda^4\Delta\lambda]\}/\{\sum[F_d(\lambda)\Delta\lambda]\} \quad (10)$$

where, F_d and $\varepsilon_a(\lambda)$ are BSA fluorescence intensity and ETS molar absorption coefficient at λ. R_0 = 0.21 Åand r = 0.24 Å are seized at $J = 3.85 \times 10^{-15}$cm^{3}L mol^{-1} and E = 28.67%. This aggregates, energy transfer from BSA (Trp134/Trp213) to ETS had prevailed via static quenching (since $r > R_0$).

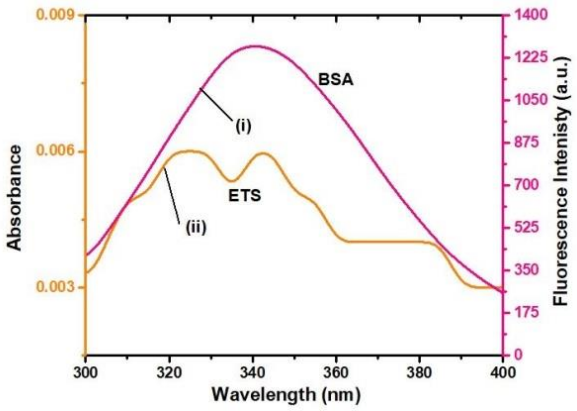

Figure 9. At 301 K overlapped spectrum: (i) bovine serum albumin (4.2×10^{-6}mol L^{-1}) fluorescence emission and (ii) etoposide (4.2×10^{-6}mol L^{-1}) UV-vis absorption.

Table 8. Different energies to etoposide−bovine serum albumin system from docking when in use Lamarckian Genetic Algorithm.

Rank	Run	ΔG^a (KJ mol^{-1})	$E_{inter-mol}{}^b$ (KJ mol^{-1})	$E_{vdw+HB+desol}{}^c$ (KJ mol^{-1})	$E_{Elec}{}^d$ (KJ mol^{-1})
1	85	−32.05	−42.05	−41.63	−0.42
2	62	−31.00	−41.00	−40.46	−0.54
3	15	−30.38	−40.38	−39.37	−1.00
4	75	−26.57	−36.53	−36.40	−0.17
5	13	−25.86	−35.86	−35.73	−0.13

[a]binding free energy, [b]bintermolecular interaction energy; sum of vander Waals energy, hydrogen bonding energy, desolvation free energy and electrostatic energy,
[c]sum of vander Waals energy, hydrogen bonding energy, and desolvation free energy, and [d]electrostatic energy

3.11. Determination of preferable binding sites.

To confirm the binding site on BSA involved with ETS, displacement experiments were done using fluorescence emission measurements in bearing site markers [22]. Equation (5) was made use for calculations of K_b values (Table 9) to BSA−ETS system in site markers (Figure 10). The acquired results certainly show that $K_b$values of ETSETS values with BSA in the presence of ibuprofen momentously decline compared to BSA−ETS only, while almost holding similar counts with and without warfarin and digitoxin. These findings recommended the sophistication of displacement interactions between ETS and ibuprofen on BSA, which elementally demonstrate that ETS binds to sub-domain IIIA of BSA.

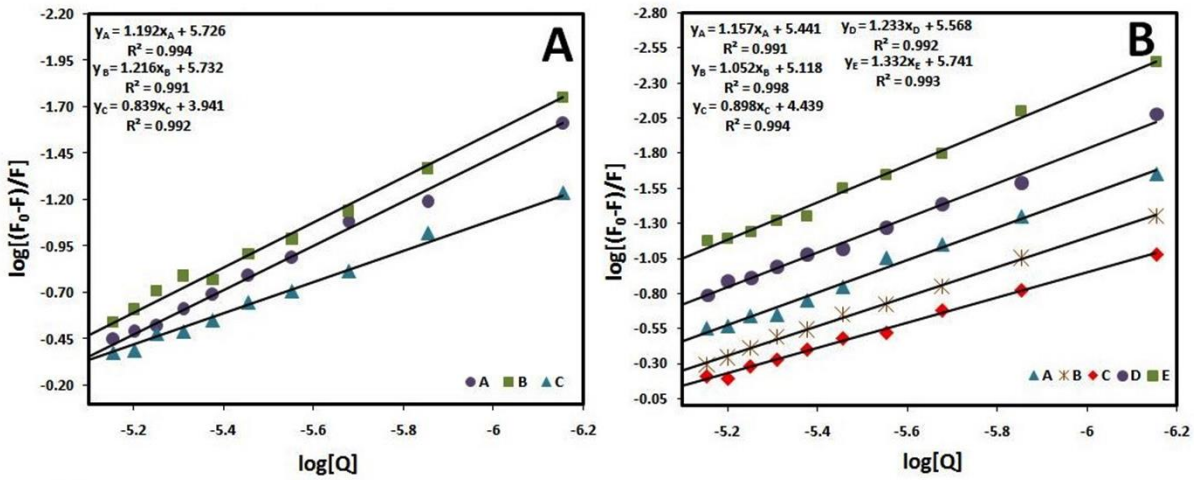

Figure 10. At 301 K, log $[(F_0 - F)/F]$ versus log$[Q]$ plot for (A) A-digitoxin, B-warfarin and C-ibuprofen (site markers) and (B) (A-Co^{2+}, B-Cu^{2+}, C-Ca^{2+}, D-Mg^{2+} and E-Fe^{2+}) (metal ions) with etoposide−bovine serum albumin system.

Table 9. Binding constant of etoposide −bovine serum albumin system at 301 K with site markers and various metal ions.

System	K_b (L mol^{-1}) [a]
BSA−ETS	$5.36 \pm 0.06 \times 10^5$
BSA−ETS −warfarin	$5.39 \pm 0.04 \times 10^5$
BSA−ETS −ibuprofen	$8.72 \pm 0.09 \times 10^3$
BSA−ETS −digitoxin	$5.32 \pm 0.01 \times 10^5$
BSA−ETS−Mg^{2+}	$3.69 \pm 0.07 \times 10^5$
BSA−ETS − Cu^{2+}	$1.31 \pm 0.04 \times 10^5$
BSA−ETS − Fe^{2+}	$5.50 \pm 0.03 \times 10^5$
BSA−ETS − Ca^{2+}	$2.75 \pm 0.06 \times 10^4$
BSA−ETS − Co^{2+}	$2.76 \pm 0.10 \times 10^5$
[a] binding constant	

3.12. Consequences of metal ions over ETS−BSA interaction.

Metal ions in plasma participate in various integral actions and pretend the drug serum albumins reactions. So the Mg^{2+}, Cu^{2+}, Fe^{2+}, $Ca^{2+,}$ and Co^{2+} ions on ETS to BSA binding constant is studied using equation (5), and values were itemized in Table 9 (Figure 10). Metal ion−ETS complex formation through metal ion bridge, this might further interact with BSA increases the ETS−BSA binding constants in the presence of Fe^{2+} ions. This may elongate when ETS remains in the blood, and hence their maximum effect enhances [23]. Presence of Cu^{2+}, Ca^{2+}, $Mg^{2+,}$ and Co^{2+} ions decrease the ETS−BSA binding constants may vary due to Cu^{2+}/ Ca^{2+}/Mg^{2+}/Co^{2+} ion and ETS competition. Therefore, the presence of Cu^{2+}/ Ca^{2+}/Mg^{2+}/Co^{2+} ion diminishes the ETS binding to BSA, resulting in ETS more doses required to achieve the essential therapeutic effect as ETS immediately cleared from the blood.

4. Conclusions

Strong binding affinity with hydrogen bonds conjointly van der Waals stabilized ETS−BSA complex at site II with appreciable distances. Apart from this, secondary, conformational with microenvironment structural alterations, BSA suffered after ETS interaction. Mg^{2+}, Cu^{2+}, Fe^{2+}, Ca^{2+} and Co^{2+} ions influenced ETS−BSA system. Future clinical ETS research and its pharmacology have great findings.

Funding

This research received no external funding.

Acknowledgments

Authors immensely express their indebtedness gratitude to the CATERS-CSIR-CLRI, Chennai for CD measurements, and IOE, Mysuru, for other instrumental facilities. Further, Manjushree Makegowda (Author) would like to extend her thanks to the Management of MMK & SDM Mahila Mahavidyalaya, Krishnamurthypuram, Mysuru for their valuable support.

Conflicts of Interest

The authors declare no conflict of interest.

References

1. Etoposide. Chemocare. http://chemocare.com/chemotherapy/drug-info/etoposide.aspx. Accessed May 29, **2020.**
2. Etoposide. Drugbank. https://www.drugbank.ca/drugs/DB00773. Accessed May 29, **2020.**
3. Etoposide. WebMD. https://www.webmd.com/drugs/2/drug-8781/etoposide-oral/details. Accessed May 29, **2020.**
4. Etoposide. Cancer Research UK. https://www.cancerresearchuk.org/about-cancer/cancer-in-general/treatment/cancer-drugs/drugs/etoposide. Accessed May 29, **2020.**
5. Sedigheh, H.; Hajar, Z.; Zaynab, M.; Mohammad, H.M. An investigation of the effect of PVP-coated silver nanoparticles on the interaction between clonazepam and bovine serum albumin based on molecular dynamics simulations and molecular docking. *Journal of Molecular Liquids* **2021**, *323*, https://doi.org/10.1016/j.molliq.2020.114915.
6. Hamid, D.; Roghaye, F.; Zeinab, M.S.; Reihaneh, B. Intermolecular investigation on interaction of two ternary copper(II) Schiff base complexes with bovine serum albumin. *Journal of Molecular Structure* **2020**, *1205*, https://doi.org/10.1016/j.molstruc.2019.127557.
7. Mhejabeen, S.; Jyoti B.; Prabhat, K.S. Haridas, P. Modulation of excited-state photodynamics of ESIPT probe 1′-hydroxy-2′- acetonaphthone (HAN) on interaction with bovine serum albumin.*Journal of Photochemistry and Photobiology A: Chemistry* **2020**, *400*, https://doi.org/10.1016/j.jphotochem.2020.112651.
8. Xi, X.; Qianqian, H.; Juanjuan, S.; Hongmei, Z.; Yanqing, W. Structural, thermal and rheological characterization of bovine serum albumin binding with sodium alginate. *Journal of Molecular Liquids* **2020**, *299*,https://doi.org/10.1016/j.molliq.2019.112123.
9. Manjushree, M.; Revanasiddappa, H.D. Spectroscopic and molecular docking elucidation to binding characteristics of bovine serum albumin with bupropion an aminoketone-medication for nicotine addiction, *European Journal of Chemistry* **2019**, *10*, 146-155, http://dx.doi.org/10.5155/eurjchem.10.2.146-155.1845
10. Tanveer, A.W.; Ahmed, H.B.; Seema, Z.; Mashooq, A.B. Abdulrahman A.A. Molecular docking and experimental investigation of new indole derivative cyclooxygenase inhibitor to probe its binding mechanism with bovine serum albumin, *Bioorganic Chemistry* **2019**, *89*, https://doi.org/10.1016/j.bioorg.2019.103010.
11. Atmanand, M.B.; Arunkumar T.B.; Naveen, M.G.; Sharanappa, T.N. Characterization of the binding and conformational changes of bovine serum albumin upon interaction with antihypertensive olmesartan medoxomil. *Journal of Molecular Structure* **2019**, *1179*,269-277, https://doi.org/10.1016/j.molstruc.2018.10.089.
12. Chuanying, Z.; Jiaxing, Z.; Hengjun, R.; Jichen, Y.; Xiaoli, W.; Xin, P. Investigation on the interaction of brazilin with bovine serum albumin using multi-spectroscopic and computational methods: Exploring the binding mechanism and inhibitory effect on amyloid aggregation. *Microchemical Journal* **2020**, *159*, https://doi.org/10.1016/j.microc.2020.105529.
13. Ali, K.; Lazhar, B.; Touhami L.; Elhafnaoui, L.; Nadjiba, Z. Spectrophotometric, voltammetric and molecular docking studies of binding interaction of N-ferrocenylmethylnitroanilines with bovine serum albumin. *Journal of Molecular Structure* **2020**, *1224*, https://doi.org/10.1016/j.molstruc.2020.129052.
14. Lakowicz, J.R. *Principles of Fluorescence Spectroscopy*. 2nd ed. Plenum Press, New York, **1999**; pp: 237–265,https://doi.org/10.1007/978-0-387-46312-4.

15. Vivek, S.; Osvaldo, Y.; César, Z.; Ashish, K.; Gurpinder, S.; Plinio, C. Protein-surfactant interactions: A multitechnique approach on the effect of Co-solvents over bovine serum albumin (BSA)-cetyl pyridinium chloride (CPC) system. *Chemical Physics Letters* **2020**, *747*, https://doi.org/10.1016/j.cplett.2020.137349.
16. Afreen, J.R.; Deepti, S.; Deepanshu K.; Mallika, P.; Anju, S.; Vinod, K.; Raman, C.; Himanshu, O. Spectroscopic and molecular modelling study of binding mechanism of bovine serum albumin with phosmet. *Spectrochimica Acta Part A: Molecular and Biomolecular Spectroscopy* **2021**, *244*, https://doi.org/10.1016/j.saa.2020.118803.
17. Vasanthakumar, A.; Ramar, R.; Malaichamy I.; Huanjun X.; Kandasamy G.M.; Yanan, G. Spectroscopic and thermodynamic studies on binding behaviour of an ionic liquid, 2 ,3 -Epoxypropyl-N-methyl-2-oxopyrrolidinium acetate, with bovine serum albumin (BSA). *Colloids and Surfaces A: Physicochemical and Engineering Aspects* **2020**, *601*, https://doi.org/10.1016/j.colsurfa.2020.124954.
18. Ross, D.P.; Subramanian, S. Thermodynamics of protein association reactions: forces contributing to stability. *Biochemistry* **1981**, *20*,3096–3102, https://doi.org/10.1021/bi00514a017.
19. Xin, Qi.; Duoxia, X.; Jinjin, Z.; Shaojia W.; Jingwei, P.; Wei, G.; Yanping, C. Studying the interaction mechanism between bovine serum albumin and lutein dipalmitate: Multi-spectroscopic and molecular docking techniques. *Food Hydrocolloids* **2021**, *113*,https://doi.org/10.1016/j.foodhyd.2020.106513.
20. Hongjin, T.; Lin, H.; Dongsheng, Z.; Chunyong, S.; Ping, S. Interaction mechanism of flavonoids on bovine serum albumin: Insights from molecular property-binding affinity relationship. *Spectrochimica Acta Part A: Molecular and Biomolecular Spectroscopy* **2020**, *239*, https://doi.org/10.1016/j.saa.2020.118519.
21. Sai, P.B.; Vipin, B.; Shailesh, B.; Anoop, K. Investigates interaction between abscisic acid and bovine serum albumin using various spectroscopic and in-silico techniques. *Journal of Molecular Structure* **2021**, *1224*, https://doi.org/10.1016/j.molstruc.2020.129018.
22. Manjushree, M.; Revanasiddappa, H.D. Interpretation of the binding interaction between bupropion hydrochloride with human serum albumin: A collective spectroscopic and computational approach. *Spectrochimica Acta Part A: Molecular and Biomolecular Spectroscopy* **2019**, *209*, 264–273, https://doi.org/10.1016/j.saa.2018.10.047.
23. Manjushree, M.; Revanasiddappa, H.D. Molecular mechanistic vision on binding interaction of triptan drug, a serotonin (5-HT1) agonist with human serum albumin through multispectral and computational assessments. *European Journal of Chemistry* **2020**, *11*, 145-155, http://dx.doi.org/10.5155/eurjchem.11.2.145-155.1971.